



17 **Abstract**

18 Short range ordered iron(III) minerals such as ferrihydrite (Fh) are ubiquitous in the environment, are key  
19 players in biogeochemical cycling, and sorb trace elements and nutrients. As such, it is important to be able  
20 to identify the presence of such minerals in natural samples. Fh is commonly observed to be X-ray  
21 amorphous and cannot be easily analyzed using X-ray diffraction, meaning that spectroscopic methods such  
22 as X-ray absorption or  $^{57}\text{Fe}$  Mössbauer spectroscopy (MBS) are necessary for accurate identification and  
23 quantification. Despite decades of research into Fh using MBS, there is discrepancy in the literature about  
24 the exact parameters applicable to the mineral when measured at liquid helium temperature. Fh is frequently  
25 fitted with either one, two or three hyperfine sextets with little interpretation applied to the meaning of each,  
26 which is problematic as a one sextet model does not account for the asymmetric lineshape frequently  
27 observed for Fh. Here, we address inconsistencies in the fitting of Fh and provide a more standardized  
28 approach to its identification by MBS. We present a systematic comparison of different fitting methods,  
29 notably based on Lorentzian and Voigt functions. We suggest that the most suitable approach to fitting pure  
30 Fh at liquid helium temperature is with two sextets (A and B) fitted using an extended Voigt based function  
31 with the ability to apply probability distributions to each hyperfine parameter. 2-Line Fh: A ( $\delta = 0.49$  mm/s;  
32  $\epsilon = 0.00$  mm/s;  $B_{\text{hf}} = 50.1$  T) and B ( $\delta = 0.42$  mm/s;  $\epsilon = -0.01$  mm/s;  $B_{\text{hf}} = 46.8$  T) 6-Line Fh: A ( $\delta = 0.50$   
33 mm/s;  $\epsilon = -0.03$  mm/s;  $B_{\text{hf}} = 50.2$  T) and B ( $\delta = 0.40$  mm/s;  $\epsilon = -0.05$  mm/s;  $B_{\text{hf}} = 47.1$  T). We interpret the  
34 two sextets to be due to either differences in the coordination environment of iron, i.e., in tetrahedral or  
35 octahedral sites, the presence of a disordered surface phase, or a combination of both. We hope that  
36 provoking a discussion on the use of MBS for Fh will help develop a greater understanding of this mineral,  
37 and other short range ordered iron minerals, which are so important in environmental processes.

38

## 39 **Introduction**

40 Nanocrystalline Fe(III) oxyhydroxide mineral phases such as ferrihydrite (Fh) are ubiquitous in the  
41 environment and constitute a major component of the global bioavailable iron pool (Jambor and Dutrizac,  
42 1998). Many biogeochemical processes such as microbial Fe cycling directly involve Fh. For example,  
43 Fe(III)-reducing microorganisms can use Fh as a terminal electron acceptor, leading to the production of  
44 Fe(II), which further transforms Fh to other iron mineral phases such as goethite, magnetite, or siderite (Han  
45 et al., 2020; Hansel et al., 2003). On the other half of the Fe cycle, Fe(II)-oxidizing bacteria, which use  
46 iron(II) as an electron donor, can precipitate Fh in soils and sediments (Kappler et al., 2021; Kappler and  
47 Straub, 2005). Interactions between Fh and organic matter have also provoked much research, especially  
48 with regard to how OM-Fh complexes can undergo transformation to other mineral phases through reaction  
49 with  $\text{Fe}^{2+}_{\text{aq}}$ , protection of OM from degradation, and on the stabilization of Fh towards further transformation  
50 (ThomasArrigo et al., 2018; Zhou et al., 2018).

51 Despite its prevalence in nature, the structure of ferrihydrite remains a point of controversy, with several  
52 different models proposed. Fh is typically referred to as either being 2-Line or 6-Line based on the number  
53 of peaks observed when analysed using X-ray diffraction (XRD). However, the Fh's nanoparticulate  
54 character and short-range-order mean that analysis of either type of Fh using (XRD) can be problematic  
55 (Cismasu et al., 2011). A study by Eggleton and Fitzpatrick suggested up to 36% Fe to be in tetrahedral  
56 coordination in Fh (Eggleton and Fitzpatrick, 1988). This finding was followed up using  $^{57}\text{Fe}$  Mössbauer  
57 spectroscopy (MBS) to investigate 6-Line Fh at room temperature and concluded that the spectrum could  
58 be equally well fitted if Fh contained either 0% or 25% tetrahedral Fe (Cardile, 1988). A study by Pankhurst  
59 and Pollard of both 2-Line and 6-Line Fh applied a magnetic field between 0-9 T, and were able to see clear  
60 splitting of the Fh spectra resulting in changes to the main hyperfine parameters isomer shift ( $\delta$ ), quadrupole  
61 shift ( $\epsilon$ ), and hyperfine magnetic field ( $B_{\text{hf}}$ ), which indicated the presence of more than one Fe spectral  
62 component (Pankhurst and Pollard, 1992). The authors determined these phases to be due to the existence  
63 of ferrimagnetism and antiferromagnetism for 2-Line and 6-Line Fh, respectively. Ultimately, the continued

64 use of MBS to study Fh has not been able to conclusively prove or disprove the presence of tetrahedral Fe  
65 (Guyodo et al., 2006). Some of the more recent developments in understanding the structure of Fh have  
66 focused on the use of X-ray scattering to derive and model pair distribution function (PDF). Using this  
67 method, Michel has argued for a structural model consisting of a unit cell with 12 Fe atoms in octahedral  
68 coordination and 1 Fe atom in tetrahedral coordination (Michel et al., 2010). This model is also supported  
69 by others who have used soft X-ray spectroscopy to study the crystal field environment of Fe in Fh (Peak  
70 and Regier, 2012). In contrast, (Drits et al., 1993) and (Manceau, 2011) have favoured an entirely  
71 octahedrally coordinated Fe model, although the Michel model appears to have gained the most widespread  
72 acceptance in recent years and several papers have further supported the presence of tetrahedral iron in Fh  
73 (Gilbert et al., 2013; Guyodo et al., 2012; Harrington et al., 2011; Maillot et al., 2011; Weatherill et al.,  
74 2016).

75 Outside of a description of iron's coordination number in Fh, the use of MBS appears to be rapidly growing  
76 in the study of Fh in environmental systems. One of the main strengths of MBS is its ability to distinguish  
77 Fe oxidation states in paramagnetic samples due to the distinctive hyperfine parameters corresponding to  
78 Fe(II) and Fe(III) phases, which typically have high and low isomer shift and quadrupole splitting values  
79 respectively (Murad, 2010). Furthermore, differences between the magnetic ordering temperature of  
80 different iron minerals provides the opportunity to characterize differences in the crystallinity in Fh  
81 coprecipitates in natural samples by collection of spectra at different temperatures (Chen and Thompson,  
82 2021). The use of MBS for mineral identification can prove challenging as many non-unique solutions may  
83 exist meaning that different analysts could come up with vastly different results if no predetermined criteria  
84 are agreed between them with the identification of Fh being no exception. One of the most striking problems  
85 in establishing fitting routines for Fh is the fact that there is a frequent interchange between either a one,  
86 two or sometimes three sextet approach. In well-established and often cited literature, such as (Cornell and  
87 Schwertmann, 2003), it is reported that only one sextet is needed for Fh when measured at liquid helium  
88 (LHe) temperature with hyperfine parameters (isomer shift  $[\delta] = 0.24^{\#}$ ; quadrupole shift  $[\varepsilon] = -0.01$ ;  
89 hyperfine magnetic field  $[B_{hf}] = 47$ ) for 2-Line and ( $\delta = 0.25^{\#}$ ;  $\varepsilon = -0.06$ ;  $B_{hf} = 50$ ) for 6-Line Fh (<sup>#</sup>Note that

90 *the low  $\delta$  values reported indicates that the spectrometer was likely calibrated with something other than*  
91 *Fe(0)).* In contrast, an earlier study used two sextets to fit Fh with hyperfine parameters (Sextet 1:  $\delta = 0.49$ ;  
92  $\epsilon = -0.37$ ;  $B_{\text{hf}} = 45.3$ , Sextet 2:  $\delta = 0.49$ ;  $\epsilon = 0.01$ ;  $B_{\text{hf}} = 45.9$ ) (Murad, 1988). These parameters diverge  
93 considerably from values reported in most other studies and might even suggest that the sample was  
94 incorrectly identified as Fh. This confusing situation of a differing number of sextets to use is not isolated,  
95 with many one sextet (Eusterhues et al., 2008) or two sextet (Pankhurst and Pollard, 1992; Schwertmann et  
96 al., 2005) studies published. More recently, Dehouck et al. used a three-sextet approach to fit a range of  
97 samples used to simulate the potential transformation of ferrihydrite on the surface of Mars (Dehouck et al.,  
98 2017). In that study, a three-sextet fit provided the most satisfactory goodness of fit, but no interpretation of  
99 each site was suggested. In general, the absence of a standardized approach to fitting Fh or Fh-like  
100 Mössbauer spectra can lead to ambiguous interpretations, which could in principle lead to different  
101 spectroscopists reporting vastly different results even when given the same dataset.

102 Coupled to this issue of how many sextets to use in the fitting is the selection of the model used to fit the  
103 data. A large range of software is available for Mössbauer analysis, however, almost all of them make use  
104 of similar approaches to fitting data, namely minimizing the difference between the model and the data by  
105 varying hyperfine parameters. Many of the models used for fitting environmental samples are based on a  
106 superposition of Lorentzian distribution to obtain good initial estimates of hyperfine parameters. However,  
107 natural samples, or samples with a distribution of individual hyperfine parameters, for instance because of  
108 a distribution of particle sizes, are poorly fitted by this most basic approach. Alternatively the Voigt (or  
109 pseudo-Voigt) profile (Prescher et al., 2012; Rancourt and Ping, 1991), which is defined by a convolution  
110 between Lorentzian and Gaussian distributions, can be used to determine the probability distribution of one  
111 primary hyperfine parameter, which in the case of a sextet is the magnetic hyperfine field  $B_{\text{hf}}$ . Voigt fitting  
112 yields an additional parameter, which describes the standard deviation of the hyperfine field ( $\sigma_{B_{\text{hf}}}$ ). In a  
113 further extension to the Voigt based fitting approach, Lagarec and Rancourt later developed a method of  
114 obtaining the probability distribution of all three hyperfine sites  $\delta$ ,  $\epsilon$ , and  $B_{\text{hf}}$  (Lagarec and Rancourt, 1997).  
115 This extended Voigt based fitting provides more flexibility in terms of fitting spectra and is especially

116 helpful for fitting environmental samples that are often comprised of a range of particle sizes. Using different  
117 models such as Lorentzian or Voigt can yield diverging results when fitting Fe minerals such as Fh, and so  
118 making an appropriate decision about which to use is critical to the success of the analysis. Furthermore,  
119 the higher number of fitting parameters available for more complex models such as xVBF can increase the  
120 likelihood of overinterpreting a spectrum. This is especially true for natural samples, which often contain  
121 multiple minerals (e.g., goethite, ferrihydrite, hematite, etc.) with overlapping features that are not easily  
122 constrained when the number of fitting parameters increases.

123 Here we present a study aimed at addressing the asymmetry of the Fh spectrum when measured at low  
124 temperature (Murad, 1988), which has been often overlooked in the more recent literature especially in  
125 environmental sciences. We place particular emphasis on addressing a largely ignored asymmetry of the Fh  
126 spectrum when measured at low temperature. This asymmetry cannot be explained by a one sextet fitting  
127 approach alone and provided the original motivation to investigate Fh in more detail. We present a  
128 comprehensive comparison of Fh Mössbauer data fitted using either one, two, three sextets and compare the  
129 results obtained when using Lorentzian, Voigt or extended Voigt based models. We also re-evaluate Fh  
130 produced by a marine, Fe(II)-oxidizing bacteria and investigate how the hyperfine parameters of Fh change  
131 as function of synthesis pH. Overall, we hope that this study will provide a more accurate approach to  
132 analyzing Fh in synthetic and natural samples.

## 133 **Materials and Methods**

### 134 Mineral synthesis

135 Several different types of ferrihydrite were prepared for these experiments including:

136 i) **6-Line Fh** was synthesised by addition of  $\text{Fe}(\text{NO}_3)_3 \cdot 9\text{H}_2\text{O}$  (20 g) into preheated (75°C) deionised  $\text{H}_2\text{O}$   
137 and rapidly stirred (Schwertmann and Cornell, 2000). The solution was placed in an oven at 75°C for 10  
138 minutes and then rapidly cooled by plunging into ice water. The solution containing precipitate was then

139 transferred into a dialysis bag and dialysed for 3 days, replacing water several times per day. The final  
140 precipitate was then collected and freeze dried.

141 ii) **2-Line Fh** was prepared by reaction of  $\text{Fe}(\text{NO}_3)_3 \cdot 9\text{H}_2\text{O}$  (40 g) with KOH (1 M) until pH 7.0  
142 (Schwertmann and Cornell, 2000). The material was centrifuged (7500 rpm; 10 min) and washed in  
143 ultrapure  $\text{H}_2\text{O}$  (Milli-Q) to remove nitrate ions, with washing repeated three times. 2-Line Fh was then  
144 freeze dried.

145 iii) **Biogenic Fh** was prepared and analysed by MBS during a published project by Swanner et al. (Swanner  
146 et al., 2015). In that study, a marine phototrophic Fe(II) oxidizer *Rhodovulum iodosum* produced short-range  
147 ordered Fe(III) (oxyhydr)oxide minerals, which were harvested after several days of incubation, and air  
148 dried in an anoxic glovebox.

149 iv) **pH-dependent Fh** was prepared according to the approach of 2-Line Fh, (Schwertmann and Cornell,  
150 2000), however, samples were collected for analysis at various pH values (between pH 3 – 11) during the  
151 addition of KOH. Samples were not freeze dried, and instead prepared for MBS by filtration (see below).  
152 Zeta potentials were measured at each corresponding pH value using a Zetasizer Nano ZSP (Malvern  
153 Instruments, UK).

#### 154 $^{57}\text{Fe}$ Mössbauer spectroscopy (MBS)

155 Freeze dried samples (2-Line and 6-Line Fh) were loaded as dried powders into Plexiglas holders (1 cm<sup>2</sup>)  
156 and sealed inside an airtight bottle. Liquid suspended mineral precipitates (biogenic Fh and pH-dependent  
157 Fh) were passed through a filter (0.45  $\mu\text{m}$ , mixed cellulose esters, Millipore) and then sealed between two  
158 layers of adhesive polyimide film (Kapton) and sealed in a Schott bottle. Samples were frozen at -20°C  
159 whilst still in a  $\text{N}_2$  atmosphere and stored for up to 1 month prior to loading into the instrument.

160 Each sample was inserted into a closed-cycle exchange gas cryostat (Janis cryogenics) with spectra  
161 measured either 295 K, 77 K or 5 K using a constant acceleration drive system (WissEL) in transmission  
162 mode with a  $^{57}\text{Co}/\text{Rh}$  source and calibrated against a 7  $\mu\text{m}$  thick  $\alpha$ - $^{57}\text{Fe}$  foil measured at room temperature.

163 Spectra were analysed using Recoil (University of Ottawa) by applying either the Lorentzian model, the  
164 Voigt Based Fitting (VBF) routine (Rancourt and Ping, 1991), or the extended Voigt Based Fitting  
165 (xVBF) routine (Lagarec and Rancourt, 1997). The main difference between VBF and xVBF fitting  
166 routines is the ability for the latter to include a distribution of the hyperfine parameters  $\delta$ ,  $\epsilon$  and  $B_{\text{hf}}$   
167 (denoted  $\sigma(\delta)$ ,  $\sigma(\epsilon)$ ,  $\sigma(B_{\text{hf}})$  respectively). In contrast, the VBF fitting routine only permits a distribution of  
168  $B_{\text{hf}}$  ( $\sigma(B_{\text{hf}})$ ). The half width at half maximum (HWHM) was fixed to a value of 0.125 mm/s for all  
169 samples, which was determined to be the inner line broadening of the calibration foil at room temperature.  
170 Table S1 denotes the parameters that were unconstrained and constrained during fitting. Recoil offers the  
171 possibility of adding more than one component per sextet, having equal isomer shifts and quadrupole  
172 shifts, but with a distribution of hyperfine fields. We applied multi-component fitting for 2-Line Fh with  
173 the xVBF model as described below (Figure S2).

174



175 **Results**

176 **2-Line and 6-Line Fh**

177 The raw data without fits for the MBS for 2-Line and 6-Line Fh collected at 295 K, 77 K, and 5 K are shown  
178 in **Figure 1**. At 295 K, both samples exhibit superparamagnetic behavior as indicated by the clear dominance  
179 of a doublet, with no evidence for a sextet. Some asymmetry is notable in the 6-Line Fh sample with the left  
180 peak of the doublet having lower intensity than the right peak. The spectra show that 2-Line Fh remained  
181 superparamagnetic until below 77 K as indicated by the absence of a clear sextet. In comparison, 6-Line Fh  
182 was already undergoing magnetic ordering above 77 K, as indicated by the presence of a partially ordered  
183 sextet at 77 K. At 5 K, the asymmetry of both 2-Line and 6-Line Fh is slight, but obvious, with the first and  
184 six lines of each sextet having a clear difference in intensity. The magnitude of the asymmetry ( $\alpha$ ) is  
185 calculated according to equation 1.

186 
$$\alpha (\%) = \frac{\Delta_6}{\Delta_1} * 100 \quad (1)$$

187 Where  $\Delta_1$  and  $\Delta_6$  correspond to the difference between the baseline and maximum amplitude of peaks 1 and  
188 6 respectively. The asymmetry parameter is calculated as 7.4 and 10.6% for 2-line and 6-line FH,  
189 respectively. These values of  $\alpha$  represent clear evidence that the spectra do not obey the symmetrical line  
190 intensities (i.e., 3:2:1:1:2:3) expected of single magnetic sublattice such as a pure powdered mineral phase  
191 (Murad, 2013).

192 Further evidence of the asymmetry in 2-Line and 6-Line spectra collected at 5 K is shown in **Figure 2**. The  
193 figure shows the results from fitting both spectra with between one and three sextets with the Lorentzian,  
194 Voigt and extended Voigt models available in Recoil (Lagarec and Rancourt, 1998). With only a one sextet  
195 fit, each model provides almost identical  $\delta$ ,  $\varepsilon$ , and  $B_{hf}$  for both 2-Line and 6-Line Fh (**Table 1**).

196 In the two site approach, the site with larger hyperfine magnetic field is denoted A (average  $B_{hf}$  = 50.2 T for  
197 all models), whereas the sextet with narrower hyperfine magnetic field is denoted B (average  $B_{hf}$  = 47.5 T  
198 for all models). With the two sextet approach, clearer differences between 2-Line and 6-Line Fh begin to

199 emerge, specifically in the relative abundances of each sextet. The 2-Line Fh B site sextets have spectral  
200 areas of  $46.5 \pm 1.1\%$ ,  $52.9 \pm 0.6\%$ ,  $45.2 \pm 4.1\%$  for Lorentzian, VBF and xVBF modelling approaches,  
201 respectively. In comparison, the 6-Line B sextets have spectral areas of  $43.2 \pm 2.5\%$ ,  $46.6 \pm 1.6\%$  and  
202  $36.5 \pm 4.4\%$  for Lorentzian, VBF and xVBF modelling approaches, respectively. As sextet B has the lowest  
203 hyperfine field, we suggest that it could correspond to a different magnetic sublattice with different Fe-O-  
204 Fe distances, or to a more disordered phase than sextet A (see discussion). Based on visual inspection even  
205 though the asymmetry has been addressed, the Lorentzian model is only able to fit the data poorly, with the  
206 xVBF model (that enables the fitting of probability distributions for  $\delta$ ,  $\varepsilon$  and  $B_{\text{hf}}$  compared to VBF model,  
207 which only fits a probability distribution for  $B_{\text{hf}}$ ) providing the most satisfactory fit.

208 The three sextet approach is more complex with an additional sextet C required, which has the lowest  
209 hyperfine magnetic field of all sextets with average  $B_{\text{hf}} = 46.3$  T. The relative area of this third sextet ranges  
210 from  $23.1 \pm 2.3\%$  to  $38.7 \pm 8.6\%$  indicating a wide range of potential solutions. Furthermore, the C sextets all  
211 have larger  $\sigma(B_{\text{hf}})$  compared to either the A or B sextets (Table 1).

212 **Figure 3** shows a comparison of residuals (i.e., difference between data and model) as well as the goodness  
213 of fit (reduced  $\chi^2$ ) for each model used. The goodness of fit is not necessarily the best measure of fitting  
214 accuracy as it is influenced by the signal to noise ratio. For instance, if signal to noise ratio is high with an  
215 almost flat background region, reduced  $\chi^2$  is likely to be much higher than if the exact same sample was  
216 measured at a lower concentration and had poorer signal to noise ratio. However, reduced  $\chi^2$  can still provide  
217 a rule of thumb for how well the model fits the data and in general, spectral fits with reduced  $\chi^2 \leq 1$  are  
218 considered to provide a good representation of the data. The residuals shown in Figure 3a confirm the  
219 expectations from visual inspection of the data shown in Figure 2 that a one sextet approach to fitting is  
220 unable to accurately describe the data with several peaks and troughs that are characteristic of an  
221 insufficiently fitted spectrum. These peaks and troughs are visible for all models apart from xVBF fitted  
222 with either two or three sextets.

223 Figure 3b shows a comparison between the goodness of fits for all fitted spectra. The reduced  $\chi^2$  is above 5  
224 for every 2-Line Fh model fitted with only one sextet. 6-Line Fh has reduced  $\chi^2$  above 5 for all one sextet  
225 models except the xVBF model, which has reduced  $\chi^2 = 4.7$ . As the number of sextets used for fitting  
226 increases, reduced  $\chi^2$  decreases. However, the xVBF model consistently provides the best results, though  
227 this is also due to the fact that there are more parameters available to vary than in the other fitting models.

228 In order to evaluate if a single sextet, multi-component fit would yield a better agreement with the data we  
229 also fitted 2-Line Fh data using the xVBF model with a single sextet and increasing number of hyperfine  
230 field components. This enabled a non-gaussian distribution of  $B_{\text{hf}}$  and is often used during fitting samples  
231 with non-homogenous size distributions (Figure S2). Increasing the number of components led to a decrease  
232 in the amplitude of the peaks and troughs in the residual, indicating an improvement of the fit. However,  
233 the hyperfine parameter histograms (Figure S2 U-Y) show deviations from a symmetric, or even skewed  
234 profile. When 1 sextet and 3 components are used, the histogram has two peaks. Furthermore, closer  
235 inspection of peak 1 (Figure S2 H) and peak 6 (Figure S2 M) suggest that the fit does not match up well  
236 with the data. In contrast, fitting with 2 or 3 sextets and only 1 component (Figure S2 D & E) show close  
237 agreement between the data and fit, residuals with little pattern, and clear probability distributions.

### 238 **Biogenic Fh**

239 To evaluate if the asymmetry was confined to chemically synthesised, freeze dried Fh, we re-evaluated data  
240 measured for biogenic Fh from a marine phototrophic Fe(II)-oxidizing bacterium, *Rhodovulum iodosum*,  
241 which was collected for a study published in 2015 (Swanner et al., 2015) (**Figure 4**). This data was originally  
242 fit with one xVBF sextet with  $\delta = 0.49$  mm/s,  $\varepsilon = -0.06$  mm/s,  $B_{\text{hf}} = 49.4$  T, reduced  $\chi^2 = 1.4$ . While this  
243 original fitting provided a reasonable assessment of the data with an acceptable goodness of fit, a closer  
244 evaluation of the raw data reveals some asymmetry ( $\alpha = 4.9\%$ ), and the residual reveals peaks and troughs  
245 similar to either 2-Line or 6-Line Fh (Figure 3A) when fitted with just one sextet, though not as intense.  
246 When the spectrum was re-evaluated with two xVBF sextets, the asymmetry was no longer visible, and the  
247 residual showed a more uniform pattern (Table S1; reduced  $\chi^2 = 0.6$ ). The hyperfine parameters for sextet

248 A were  $\delta = 0.50 \pm 0.01$  mm/s,  $\epsilon = -0.07 \pm 0.01$  mm/s,  $B_{\text{hf}} = 49.9 \pm 0.08$  T, R.A. =  $57 \pm 6\%$ , with sextet B having  
249  $\delta = 0.45 \pm 0.03$  mm/s,  $\epsilon = -0.04 \pm 0.02$  mm/s,  $B_{\text{hf}} = 47.0 \pm 0.7$  T, R.A. =  $43 \pm 6\%$  both of which were consistent  
250 with results obtained for 2-Line and 6-Line Fh when fitted with two sextets and the xVBF model. Comparing  
251 these hyperfine parameters with those determined for synthetic Fh it is difficult to determine if the biogenic  
252 sample is closer to 2-Line or to 6-Line Fh and so is best described as simply biogenic Fh (Figure S3). Even  
253 though the differences between the hyperfine parameters appear relatively minor, a better understanding of  
254 the accurate structure of Fh can help to explain its importance in biogeochemical systems such as these.

### 255 **Analysis of Fh synthesized at different pH**

256 We performed an additional experiment to evaluate Fh using MBS focused on the formation of Fe(III)-  
257 precipitates using the standard protocol used to synthesize Fh, but with samples collected at different pH  
258 (**Figure S1; Table S1**). These samples were collected during the precipitation of 2-Line Fh and then  
259 subsequently analysed at 5 K. **Figure 5** shows a comparison between different hyperfine parameters as a  
260 function of Fh synthesis-pH obtained by fitting each spectrum with two xVBF sextets. The data show clear  
261 distinction between the two sextets at all pH. The isomer shift exhibits a linear correlation with synthesis-  
262 pH, with sextet B showing a stronger negative linear correlation than sextet A suggesting that the effect of  
263 pH was more strongly associated with the B sextet. The magnetic hyperfine field of both sites appear to  
264 increase as a function of pH. The quadrupole shift shows some positive correlation to the Fh synthesis pH.  
265 Finally, the relative abundance of sextet A and sextet B appears to change as a function of pH, with the A  
266 and B sextets occupying a decreasing and increasing proportion of the spectral area, respectively, as  
267 synthesis pH increases.

268 These data indicate that the properties of Fh change as a function of synthesis pH, which as far as we are  
269 aware, has not been previously shown by MBS. Potentially, these differences might also reflect a change in  
270 the Fh surface properties, for example zeta potential (ZP) which was also measured for these samples.  
271 Changes to the zeta potential occur as a result of a change in the surface charge of the ferrihydrite which is  
272 positive below the point of zero charge (PZC) and negative above (Li et al., 2015). **Figure 6** shows a side-

273 by-side comparison of changes in ZP,  $\delta$  (Sextet A),  $\delta$  (Sextet B) as a function of pH (both y-axes for  $\delta$  span  
274 a range of 0.025 mm/s). Interestingly, the  $\delta$  of both A and B sextets appear to change just before the point  
275 of zero charge (PZC; pH = 8.3), with the B sextet exhibiting the largest change. The changes are relatively  
276 small, however, this provides support to the idea that the B sextet corresponds to a surface bound site.

## 277 **Discussion**

278 When fitting Mössbauer data, it is best practice to find an appropriate fit with an acceptable reduced  $\chi^2$  using  
279 the least number of sextets or doublets. This is necessary to prevent “over fitting”, which can lead to a poor  
280 interpretation of the sample (Hargraves et al., 1990). In the 2-Line Fh and 6-Line Fh spectra (Figure 1-3;  
281 Table 1) the smallest reduced  $\chi^2$  was consistently achieved when using the xVBF model. This is particularly  
282 evident from inspection of the residuals though smaller reduced  $\chi^2$  is likely to be also due to higher number  
283 of parameters available for xVBF compared to the Lorentzian or VBF fitting approaches. The issue of  
284 asymmetry was resolved by fitting with two sextets for 2-Line and 6-line Fh with reduced  $\chi^2 = 3.2$  and  
285 reduced  $\chi^2 = 1.14$  respectively. Reduced  $\chi^2$  remained above 1 for 2-Line Fh (reduced  $\chi^2 = 2.4$ ) even when a  
286 three sextet xVBF model was used. 6-Line Fh had reduced  $\chi^2 = 0.86$  when fitted with a three sextet xVBF  
287 model. Even though a three sextet approach provides the best fit, the correct assignment of each site becomes  
288 more and more complex. We suggest that the two sextet approach is the safest option and still allows the  
289 physical interpretation of each site.

290 In order for the two sextet approach to be accepted, a better understanding of each site needs to be  
291 considered. We hypothesise that a two sextet model can be explained by either (I) coordination of iron atoms  
292 in tetrahedral and octahedral sites, (II) surface disorder, or (III) a combination of the two.

### 293 I) Tetrahedral and octahedral sites

294 The structure of ferrihydrite remains under debate, with several different models proposed for its structure.  
295 Eggleton and Fitzpatrick suggest up to 36% Fe to be in tetrahedral coordination in Fh (Eggleton and  
296 Fitzpatrick, 1988). Peak and Regier (2012) suggested as much as 30-40% tetrahedral iron, which was in

297 close agreement with other X-ray spectroscopic results (Guyodo et al., 2012; Maillot et al., 2011). Michel  
298 et al. argued for an ideal structure which contained 20% tetrahedral Fe (Michel et al., 2007), but that  
299 vacancies may mean that some tetrahedral sites are empty leading to a unit cell with 12 Fe atoms in  
300 octahedral coordination and 1 Fe atom in tetrahedral coordination (i.e., 7.7% tetrahedral Fe) (Michel et al.,  
301 2010). Previous studies have separated tetrahedral and octahedral coordinated iron on the basis of isomer  
302 shift in MBS spectra, with lower  $\delta$  being more indicative of tetrahedral iron (Cuadros et al., 2019; Kuzmann  
303 et al., 2003). The average  $\delta$  for the A and B sextets shown when fitted with 2 sextets (Table 1) were  
304  $0.503 \pm 0.036$  mm/s and  $0.410 \pm 0.045$  mm/s for 2-Line Fh respectively. For 6-Line Fh, A and B sextets had  
305  $\delta$  of  $0.508 \pm 0.021$  mm/s and  $0.409 \pm 0.045$  mm/s respectively (average is based on all models with errors  
306 calculated as the standard deviation from the mean). This would suggest that the B site could correspond to  
307 tetrahedral iron in ferrihydrite. However, the attempt to detect tetrahedral Fe(III) in Fh by Mössbauer is not  
308 new, and indeed faces several obstacles. As already outlined in the introduction section, the use of  
309 Mössbauer for identification of tetrahedral and octahedral sites has been previously rejected. Because  
310 tetrahedral Fe contents are frequently low, the uncertainty associated with the correspondingly low-intensity  
311 peaks in the Mössbauer spectra is high. Furthermore, there is overlap between the low-energy lines (low-  
312 velocity values) of tetrahedral Fe(III), and octahedral Fe(III) (Coey et al., 1984; Rancourt et al., 1992),  
313 making it difficult to identify tetrahedral Fe(III) and quantify it. However, considering our data, and  
314 assuming the Eggleton and Fitzpartick model in which 36% of the Fe in 6-Line Fh is in tetrahedral  
315 coordination, this would line up precisely with our reported values for the B sextet when fitted with a two  
316 sextet xVBF model (Table 1). Considering our observation that the isomer shift of sextet B varies with pH  
317 (Figure 6), that would raise the question of how pH influences tetrahedral Fe(III)? Alternatively, if we  
318 assume the Michel model to be correct, then this would imply ~8% of the Fe is tetrahedrally coordinated.  
319 Looking at the two sextet model the relative abundance of A vs. B sextets far exceed this value and it is  
320 unlikely that such a minor component would be discernible in the spectra. Even in the three sextet xVBF  
321 model the relative abundances of A, B and C sextets are much greater than this value. These conflicting

322 structural interpretations of Fh mean that we cannot explain the asymmetry as being due to the presence of  
323 tetrahedral iron within the 2-Line and 6-Line Fh.

324 II) Surface disorder

325 The effect of surface disorder in ultrafine nanoparticles has been considered for iron (oxyhydr)oxides  
326 (Dormann et al., 1999; Mørup, 1990; Tronc et al., 2000) and is potentially important in Fh (Hiemstra, 2013).  
327 Typically, the primary particles of 2-Line Fh are estimated to have a size of ca. 3 nm, compared to 6-Line  
328 Fh which has an average diameter of 2-6 nm (Schwertmann and Cornell, 2000). We did not independently  
329 verify the particle size of the Fh in this study but consider the reliability of the synthesis procedures to be  
330 satisfactory for this discussion. It was estimated by Zhao (Zhao et al., 1994) that assuming a spherical shape,  
331 ferrihydrite has a surface shell with thickness of ~2 Angstrom (equivalent to one Fe<sup>3+</sup>-O bond distance).  
332 Based on estimated particle sizes (taking d = 3 nm and d = 4 nm for 2-Line and 6-Line Fh, respectively),  
333 this would correspond to 35% and 27% of the total particle for 2-Line and 6-Line Fh, respectively (Zhao et  
334 al., 1994). These values show reasonable comparison to the relative areas of the B sites when fitted with  
335 two xVBF sextets which were 45.2% and 36.5% for 2-Line and 6-Line Fh, respectively. The effect of surface  
336 disorder was previously discussed by (Hiemstra, 2013) who suggested that the mineral core of Fh is defect  
337 free and that the size-dependent variation is surface driven. This hypothesis is analogous to our observed  
338 pH-dependent measurements in which the largest changes to the isomer shift were observed for the B sextet  
339 which we tentatively assume could correspond to the surface sites, especially as these changes line up with  
340 changes to the ZP.

341 III) Combination of the above

342 We must also consider the possibility that the asymmetry frequently observed in ferrihydrite when measured  
343 at liquid helium temperature is due to both a combination of tetrahedral Fe, and the effect of surface disorder.  
344 This would then be best fitted using a four sextet fit, to account for tetrahedral and octahedral iron in both  
345 the surface and the bulk. However, if were to consider a hypothetical Fh particle with 35% Fe atoms located  
346 at the surface and 65% Fe atoms located in the core, any tetrahedral sextets would account for 3% and 5.4%

347 of the spectral area in surface and core sites respectively (according to the Michel model). Such minor  
348 components would be difficult to distinguish against the background and it is unlikely that the mathematical  
349 fitting models used to fit the data would be able to provide accurate results. In fact, a four sextet fit was  
350 tested using the xVBF model and was unable to provide any reasonable improvement to the two or three  
351 sextet fits (data not shown).

352 Alternative explanations for a multi sextet Fh model other than those suggested above cannot be entirely  
353 ruled out. For example, a recent study considered whether 2-Line Fh was a multi-phase nanocomposite  
354 consisting of ordered nanodomains embedded in a short-range ordered ferric hydroxide matrix (Funnell et  
355 al., 2020). Another study considered the distribution of structure types in such a nanocomposite to depend  
356 on particle size, temperature and hydration (Sassi et al., 2021). The Mössbauer spectrum of such a system  
357 could conceivably require a two sextet fit, but it is unclear how different such a spectrum might look from  
358 those reported in this study and warrants further consideration.

### 359 **Implications**

360 The interpretation of the two sextet model for Fh remains open for debate and we do not consider that  
361 Mössbauer can provide a definitive answer. However, it is likely that there is at least some surface disorder,  
362 which should be accounted for that potentially influences tetrahedral iron. These results have clear  
363 implications for a wide range of studies. For example, the understanding of iron transformation in laboratory  
364 or environmental systems frequently rely on the accurate identification of Fh. In many cases, these phases  
365 are associated with other minerals such as goethite, lepidocrocite, magnetite, Fe-sulphides, phyllosilicates.  
366 Quick identification of Fh commonly relies on the observation of a single sextet with hyperfine parameters  
367 such as those previously reported (Cornell and Schwertmann, 2003). Our two-sextet model adds to the  
368 complexity of determining the mineral phase present in a natural sample. For example, if the amount of  
369 ferrihydrite in a sample is low in comparison to another mineral, which is also magnetically ordered and  
370 shares similar hyperfine parameters (e.g., goethite), then the application of two sextets for fitting ferrihydrite  
371 lead to could be ambiguities in the outcome of the fit (Chen and Thompson, 2021). In such cases, we would



372 suggest maintaining the single sextet approach, which now acts as more of an average solution to Fh. Further  
373 to this, however, samples should also be measured at several other temperatures to ease interpretation. These  
374 results also have implications on the potential complexation of Fh with organic matter (OM). It might be  
375 anticipated that any sorption of OM to Fh will be dependent on the surface of the mineral. Therefore, we  
376 anticipate that the biggest changes to the Fh structure will occur to the B sextet.

377 In summary, we recommend the most appropriate model for fitting either 2-line or 6-line ferrihydrite at  
378 liquid helium temperature is the xVBF model, with two sextets:

- 379 • 2-LineFh: A ( $\delta=0.49$  mm/s;  $\epsilon = 0.00$  mm/s;  $B_{hf} = 50.1$  T;  $\sigma(B_{hf}) = 1.51$ ) and B ( $\delta = 0.42$  mm/s;  $\epsilon =$   
380  $-0.01$  mm/s;  $B_{hf} = 46.8$  T;  $\sigma(B_{hf}) = 2.79$ )
- 381 • 6-Line Fh: A ( $\delta = 0.50$  mm/s;  $\epsilon = -0.03$  mm/s;  $B_{hf} = 50.2$  T;  $\sigma(B_{hf}) = 1.35$ ) and B ( $\delta = 0.40$  mm/s;  $\epsilon =$   
382  $-0.05$  mm/s;  $B_{hf} = 47.1$  T;  $\sigma(B_{hf}) = 2.90$ ).

### 383 **Acknowledgements**

384 Timm Bayer is thanked for preparation of pH-dependent Fh. Ying Ji and Susan Tandy are thanked for  
385 providing 2-Line and 6-Line FH. Aaron Thompson (University of Georgia), and Elizabeth Sklute (Mount  
386 Holyoke College), and other anonymous reviewers are thanked for providing critical feedback which has  
387 helped to improve the quality of the manuscript. AK acknowledges the infrastructural support by the DFG  
388 under Germany's Excellence Strategy, cluster of Excellence EXC2124, project ID 390838134.

389

## 390 References

- 391 Cardile, C. (1988) Tetrahedral Fe 3+ in Ferrihydrite: 57 Fe Mössbauer Spectroscopic Evidence. *Clays and*  
392 *Clay Minerals*, 36(6), 537-539.
- 393 Chen, C., and Thompson, A. (2021) The influence of native soil organic matter and minerals on ferrous  
394 iron oxidation. *Geochimica et Cosmochimica Acta*, 292, 254-270.
- 395 Cismasu, A.C., Michel, F.M., Tcaciuc, A.P., Tyliczszak, T., and Brown Jr, G.E. (2011) Composition and  
396 structural aspects of naturally occurring ferrihydrite. *Comptes Rendus Geoscience*, 343(2-3), 210-  
397 218.
- 398 Coey, J.M.D., Chukhrov, F.V., and Zvyagin, B.B. (1984) Cation Distribution, Mössbauer Spectra, and  
399 Magnetic Properties of Ferripyrophyllite. *Clays and Clay Minerals*, 32(3), 198-204.
- 400 Cornell, R.M., and Schwertmann, U. (2003) *The Iron Oxides Structure, Properties, Reactions, Occurrences*  
401 *and Uses*. Wiley-VCH, Weinheim, Germany.
- 402 Cuadros, J., Michalski, J.R., Dyar, M.D., and Dekov, V. (2019) Controls on tetrahedral Fe (III) abundance in  
403 2: 1 phyllosilicates. *American Mineralogist: Journal of Earth and Planetary Materials*, 104(11),  
404 1608-1619.
- 405 Dehouck, E., McLennan, S.M., Sklute, E.C., and Dyar, M.D. (2017) Stability and fate of ferrihydrite during  
406 episodes of water/rock interactions on early Mars: An experimental approach. *Journal of*  
407 *Geophysical Research: Planets*, 122(2), 358-382.
- 408 Dormann, J., Fiorani, D., Cherkaoui, R., Tronc, E., Lucari, F., d'Orazio, F., Spinu, L., Nogues, M., Kachkachi,  
409 H., and Jolivet, J. (1999) From pure superparamagnetism to glass collective state in  $\gamma$ -Fe<sub>2</sub>O<sub>3</sub>  
410 nanoparticle assemblies. *Journal of magnetism and magnetic materials*, 203(1-3), 23-27.
- 411 Drits, V., Sakharov, B., Salyn, A., and Manceau, A. (1993) Structural model for ferrihydrite. *Clay Minerals*,  
412 28, 185-207.
- 413 Eggleton, R.A., and Fitzpatrick, R.W. (1988) New data and a revised structural model for ferrihydrite.  
414 *Clays and Clay Minerals*, 36(2), 111-124.
- 415 Eusterhues, K., Wagner, F.E., Häusler, W., Hanzlik, M., Knicker, H., Totsche, K.U., Kögel-Knabner, I., and  
416 Schwertmann, U. (2008) Characterization of Ferrihydrite-Soil Organic Matter Coprecipitates by X-  
417 ray Diffraction and Mössbauer Spectroscopy. *Environmental Science & Technology*, 42(21), 7891-  
418 7897.
- 419 Funnell, N.P., Fulford, M.F., Inoué, S., Kletetschka, K., Michel, F.M., and Goodwin, A.L. (2020)  
420 Nanocomposite structure of two-line ferrihydrite powder from total scattering. *Communications*  
421 *Chemistry*, 3(1), 1-9.
- 422 Gilbert, B., Erbs, J.J., Penn, R.L., Petkov, V., Spagnoli, D., and Waychunas, G.A. (2013) A disordered  
423 nanoparticle model for 6-line ferrihydrite. *American Mineralogist*, 98(8-9), 1465-1476.
- 424 Guyodo, Y., Banerjee, S.K., Lee Penn, R., Burleson, D., Berquo, T.S., Seda, T., and Solheid, P. (2006)  
425 Magnetic properties of synthetic six-line ferrihydrite nanoparticles. *Physics of the Earth and*  
426 *Planetary Interiors*, 154(3-4), 222-233.
- 427 Guyodo, Y., Sainctavit, P., Arrio, M.A., Carvallo, C., Penn, R.L., Erbs, J.J., Forsberg, B.S., Morin, G., Maillot,  
428 F., and Lagroix, F. (2012) X-ray magnetic circular dichroism provides strong evidence for  
429 tetrahedral iron in ferrihydrite. *Geochemistry, Geophysics, Geosystems*, 13(6).
- 430 Han, X., Tomaszewski, E.J., Sorwat, J., Pan, Y., Kappler, A., and Byrne, J.M. (2020) Effect of Microbial  
431 Biomass and Humic Acids on Abiotic and Biotic Magnetite Formation. *Environmental Science &*  
432 *Technology*, 54(7), 4121-4130.
- 433 Hansel, C.M., Benner, S.G., Neiss, J., Dohnalkova, A., Kukkadapu, R.K., and Fendorf, S. (2003) Secondary  
434 mineralization pathways induced by dissimilatory iron reduction of ferrihydrite under advective  
435 flow. *Geochimica et Cosmochimica Acta*, 67(16), 2977-2992.

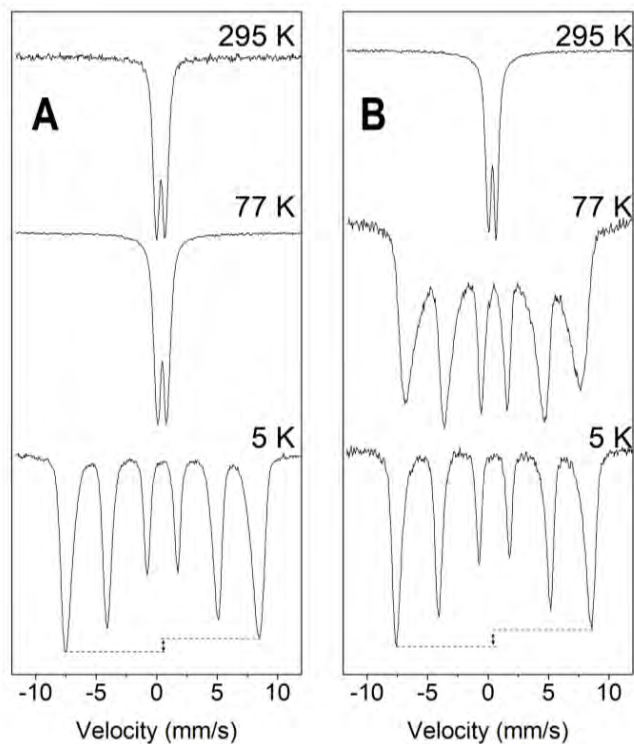
- 436 Hargraves, P., Rancourt, D.G., and Lalonde, E. (1990) Single-crystal Mössbauer study of phlogopite mica.  
437 Canadian Journal of Physics, 68(1), 128-144.
- 438 Harrington, R., Hausner, D.B., Xu, W., Bhandari, N., Michel, F.M., Brown Jr, G.E., Strongin, D.R., and  
439 Parise, J.B. (2011) Neutron pair distribution function study of two-line ferrihydrite.  
440 Environmental science & technology, 45(23), 9883-9890.
- 441 Hiemstra, T. (2013) Surface and mineral structure of ferrihydrite. Geochimica et Cosmochimica Acta, 105,  
442 316-325.
- 443 Jambor, J.L., and Dutrizac, J.E. (1998) Occurrence and constitution of natural and synthetic ferrihydrite, a  
444 widespread iron oxyhydroxide. Chemical Reviews, 98(7), 2549-2586.
- 445 Kappler, A., Bryce, C., Mansor, M., Lueder, U., Byrne, J.M., and Swanner, E.D. (2021) An evolving view on  
446 biogeochemical cycling of iron. Nature Reviews Microbiology, 19(6), 360-374.
- 447 Kappler, A., and Straub, K.L. (2005) Geomicrobiological Cycling of Iron. Reviews in Mineralogy and  
448 Geochemistry, 59(1), 85-108.
- 449 Kuzmann, E., Nagy, S., and Vértes, A. (2003) Critical review of analytical applications of Mössbauer  
450 spectroscopy illustrated by mineralogical and geological examples (IUPAC Technical Report).  
451 Pure and Applied Chemistry, 75(6), 801-858.
- 452 Lagarec, K., and Rancourt, D.G. (1997) Extended Voigt-based analytic lineshape method for determining  
453 N-dimensional correlated hyperfine parameter distributions in Mössbauer spectroscopy. Nuclear  
454 Instruments and Methods in Physics Research Section B: Beam Interactions with Materials and  
455 Atoms, 129(2), 266-280.
- 456 Lagarec, K., and Rancourt, D.G. (1998) Recoil - Mössbauer spectral analysis software for Windows.  
457 version 1.0 pp. 43.
- 458 Li, F., Geng, D., and Cao, Q. (2015) Adsorption of As(V) on aluminum-, iron-, and manganese-  
459 (oxyhydr)oxides: equilibrium and kinetics. Desalination and Water Treatment, 56(7), 1829-1838.
- 460 Maillot, F., Morin, G., Wang, Y., Bonnin, D., Ildefonse, P., Chaneac, C., and Calas, G. (2011) New insight  
461 into the structure of nanocrystalline ferrihydrite: EXAFS evidence for tetrahedrally coordinated  
462 iron (III). Geochimica et Cosmochimica Acta, 75(10), 2708-2720.
- 463 Manceau, A. (2011) Critical evaluation of the revised akdalaite model for ferrihydrite. American  
464 Mineralogist, 96(4), 521-533.
- 465 Michel, F.M., Barrón, V., Torrent, J., Morales, M.P., Serna, C.J., Boily, J.-F., Liu, Q., Ambrosini, A., Cismasu,  
466 A.C., and Brown, G.E. (2010) Ordered ferrimagnetic form of ferrihydrite reveals links among  
467 structure, composition, and magnetism. Proceedings of the National Academy of Sciences,  
468 107(7), 2787-2792.
- 469 Michel, F.M., Ehm, L., Antao, S.M., Lee, P.L., Chupas, P.J., Liu, G., Strongin, D.R., Schoonen, M.A.A.,  
470 Phillips, B.L., and Parise, J.B. (2007) The Structure of Ferrihydrite, a Nanocrystalline Material.  
471 Science, 316(5832), 1726-1729.
- 472 Mørup, S. (1990) Mössbauer effect in small particles. Hyperfine Interactions, 60(1), 959-973.
- 473 Murad, E. (1988) The Mössbauer spectrum of "well"-crystallized ferrihydrite. Journal of Magnetism and  
474 Magnetic Materials, 74(2), 153-157.
- 475 Murad, E. (2010) Mössbauer spectroscopy of clays, soils and their mineral constituents. Clay Minerals,  
476 45(4), 413-430.
- 477 Murad, E. (2013) Chapter 2.1 - Mössbauer Spectroscopy. In F. Bergaya, and G. Lagaly, Eds. Developments  
478 in Clay Science, 5, p. 11-24. Elsevier.
- 479 Pankhurst, Q., and Pollard, R. (1992) Structural and magnetic properties of ferrihydrite. Clays and Clay  
480 Minerals, 40, 268-272.
- 481 Peak, D., and Regier, T. (2012) Direct observation of tetrahedrally coordinated Fe (III) in ferrihydrite.  
482 Environmental science & technology, 46(6), 3163-3168.

- 483 Prescher, C., McCammon, C., and Dubrovinsky, L. (2012) MossA: a program for analyzing energy-domain  
484 Mössbauer spectra from conventional and synchrotron sources. *Journal of Applied*  
485 *Crystallography*, 45(2), 329-331.
- 486 Rancourt, D.G., Dang, M.Z., and Lalonde, A.E. (1992) Mössbauer spectroscopy of tetrahedral Fe<sup>3+</sup> in  
487 trioctahedral micas. *American Mineralogist*, 77(1-2), 34-43.
- 488 Rancourt, D.G., and Ping, J.Y. (1991) Voigt-based methods for arbitrary-shape static hyperfine parameter  
489 distributions in Mössbauer spectroscopy. *Nucl. Instrum. Methods Phys. Res., Sect. B*, 58(1), 85-  
490 97.
- 491 Sassi, M., Chaka, A., and Rosso, K. (2021) Ab Initio Thermodynamics Reveals the Nanocomposite  
492 Structure of Ferrihydrite.
- 493 Schwertmann, U., and Cornell, R.M. (2000) *Iron oxides in the laboratory*. John Wiley & Sons.
- 494 Schwertmann, U., Wagner, F., and Knicker, H. (2005) Ferrihydrite–Humic Associations: Magnetic  
495 Hyperfine Interactions. *Soil Sci. Soc. Am. J.*, 69(4), 1009-1015.
- 496 Swanner, E.D., Wu, W., Schoenberg, R., Byrne, J., Michel, F.M., Pan, Y., and Kappler, A. (2015)  
497 Fractionation of Fe isotopes during Fe (II) oxidation by a marine photoferrotroph is controlled by  
498 the formation of organic Fe-complexes and colloidal Fe fractions. *Geochimica et Cosmochimica*  
499 *Acta*, 165, 44-61.
- 500 ThomasArrigo, L.K., Byrne, J.M., Kappler, A., and Kretzschmar, R. (2018) Impact of Organic Matter on  
501 Iron(II)-Catalyzed Mineral Transformations in Ferrihydrite–Organic Matter Coprecipitates.  
502 *Environmental Science & Technology*, 52(21), 12316-12326.
- 503 Tronc, E., Ezzir, A., Cherkaoui, R., Chanéac, C., Noguès, M., Kachkachi, H., Fiorani, D., Testa, A., Greneche,  
504 J., and Jolivet, J. (2000) Surface-related properties of  $\gamma$ -Fe<sub>2</sub>O<sub>3</sub> nanoparticles. *Journal of*  
505 *Magnetism and Magnetic Materials*, 221(1-2), 63-79.
- 506 Weatherill, J.S., Morris, K., Bots, P., Stawski, T.M., Janssen, A., Abrahamsen, L., Blackham, R., and Shaw,  
507 S. (2016) Ferrihydrite formation: the role of Fe<sup>13</sup> Keggin clusters. *Environmental science &*  
508 *technology*, 50(17), 9333-9342.
- 509 Zhao, J., Huggins, F.E., Feng, Z., and Huffman, G.P. (1994) Ferrihydrite; surface structure and its effects on  
510 phase transformation. *Clays and Clay Minerals*, 42(6), 737-746.
- 511 Zhou, Z., Latta, D.E., Noor, N., Thompson, A., Borch, T., and Scherer, M.M. (2018) Fe (II)-Catalyzed  
512 Transformation of Organic Matter–Ferrihydrite Coprecipitates: A Closer Look Using Fe Isotopes.  
513 *Environmental science & technology*, 52(19), 11142-11150.

514

515

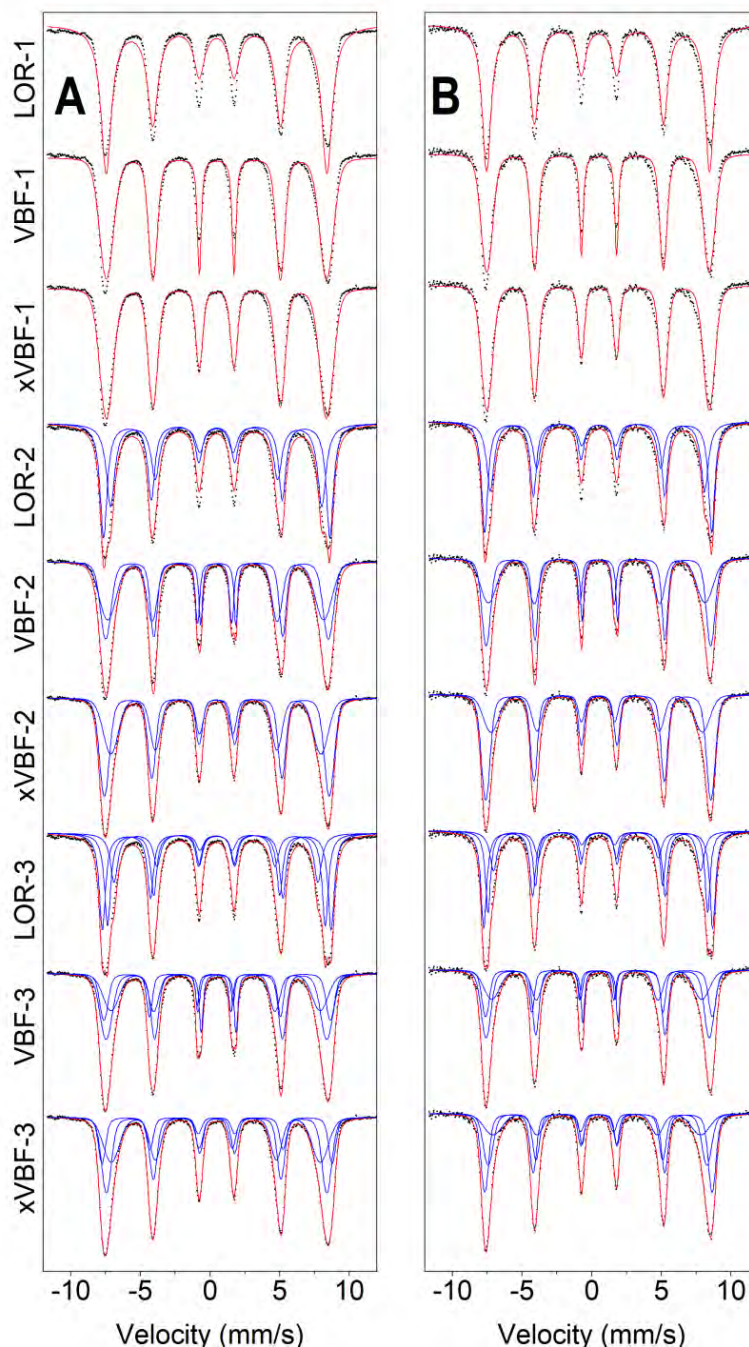
516 **Figures**



517

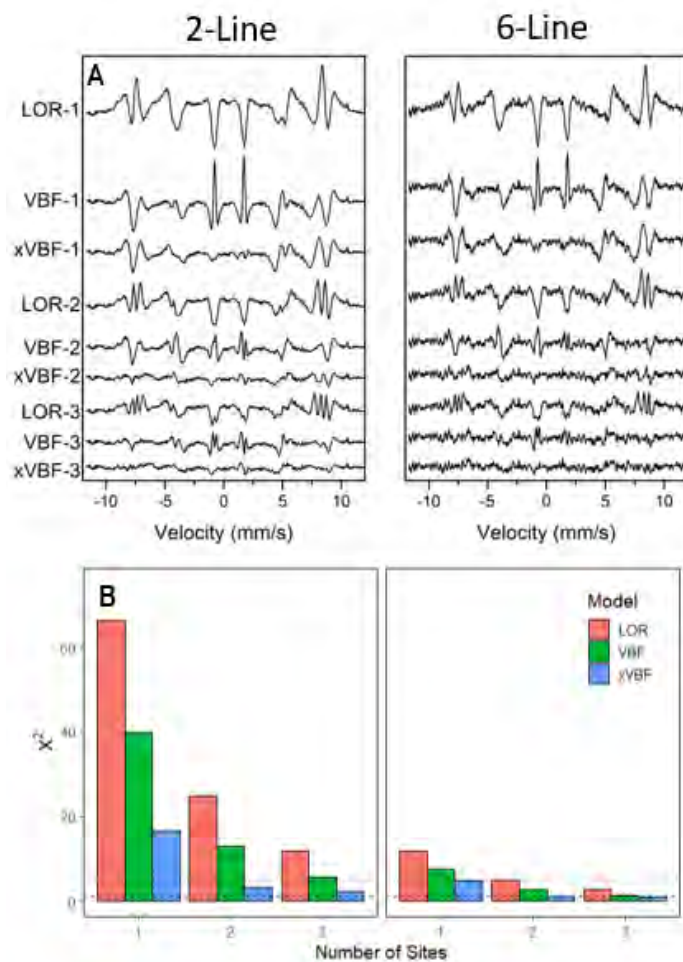
518 **Figure 1** –  $^{57}\text{Fe}$  Mössbauer data collected for (A) 2-Line Fh and (B) 6-Line Fh at 295, 77 and 5 K. The dashed line shown for  
519 the 5 K spectra indicates the asymmetry which is observable when measured at liquid helium temperature.

520



521

522 *Figure 2 – Fitting results for (A) 2-Line and (B) 6-Line FH. Data shown were fit with Lorentzian line (LOR), Voigt (VBF) and*  
523 *extended Voigt models (xVBF). -1, -2, and -3 on each label refers to one, two or three sextet fits, respectively.*



524

525

*Figure 3 – Comparison of fitting quality. (A) Residuals indicating the difference between data and fit 2 line and 6 line*

526

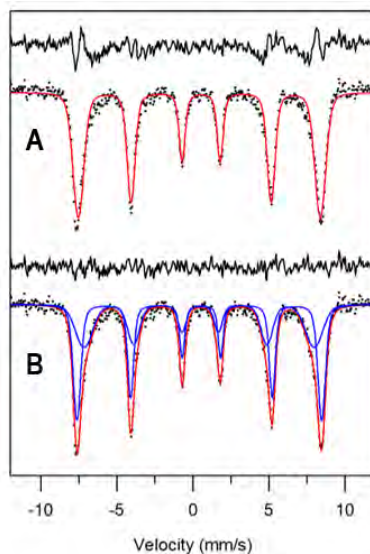
*ferrihydrate. (B) reduced  $\chi^2$  of all fitting approaches for 2-Line and 6-Line Fh. Dashed line represents reduced  $\chi^2 = 1$ , with*

527

*dotted line indicating reduced  $\chi^2 = 5$ .*

528

529

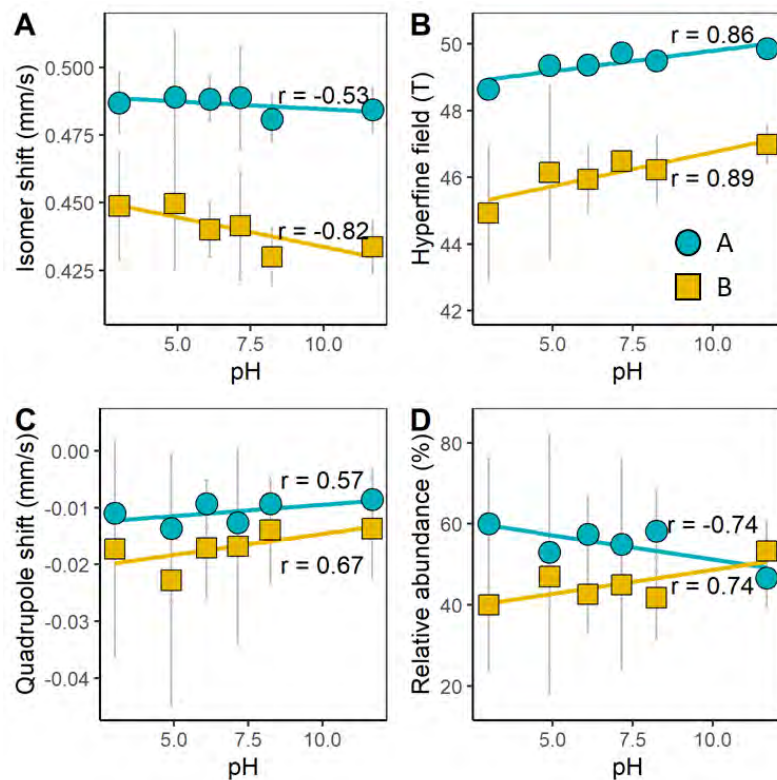


530

531 *Figure 4 – Biogenic ferrihydrite fitted with 1 sextet (A) compared with 2 sextets (B) with the xVBF fitting routine. Black lines*  
532 *indicate the residual, i.e., difference between model and data. Data from (Swanner et al., 2015) reproduced with permission*  
533 *(Copyright © 2015 Elsevier Ltd).*

534





535

536

537

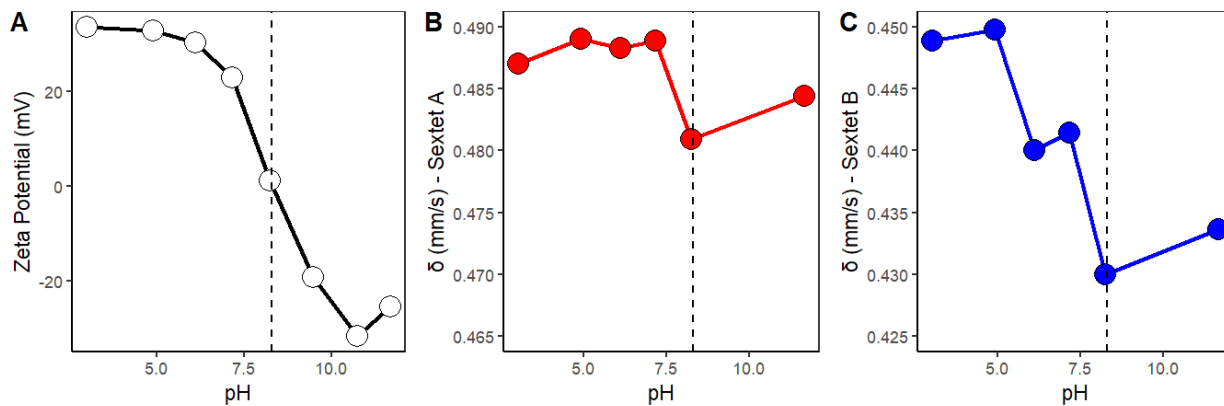
538

539

540

541

**Figure 5 – Hyperfine parameters of Fh synthesized at different pH fitted with two xVBF sextets. Turquoise lines correspond to sextet A, yellow lines to sextet B. Error bars indicate uncertainty for each parameter provided by the fitting software.**



542

543 *Figure 6 – Changes to Fh (A) zeta potential (ZP), (B) isomer shift of sextet A, and (C) isomer shift of sextet B as a function of*  
544 *synthesis pH (both y-axes for  $\delta$  span a range of 0.025 mm/s). Dashed line indicates point of zero charge (pH = 8.3).*

545

546

547 **Tables**

548 *Table 1 – Hyperfine parameters obtained for fitting 2-Line and 6-Line Fh with Lorentzian (LOR), Voigt (VBF) or extended*  
 549 *Voigt (xVBF) models. N<sub>sx</sub> – number of sextets per model, Sextet – indicates each sextet, δ – isomer shift (mm/s), σ(δ) – standard*  
 550 *deviation of the isomer shift, ε – quadrupole shift (mm/s), σ(ε) – standard deviation of the quadrupole shift, B<sub>hf</sub> – hyperfine*  
 551 *magnetic field (T), σ(B<sub>hf</sub>) – standard deviation of hyperfine magnetic field (T), w – linewidth of the Lorentzian (mm/s), R.A. –*  
 552 *relative abundance (%), red. (reduced) χ<sup>2</sup> – goodness of fit.*

Model	Sample	N <sub>sx</sub>	Sextet	δ mm/s	±	σ(δ) mm/s	ε mm/s	±	σ(ε) mm/s	B <sub>hf</sub> T	±	σ(B <sub>hf</sub> ) T	±	w mm/s	±	R.A. %	±	red. χ <sup>2</sup>
LOR	2L	1	A	0.468	0.001		-0.004	0.001		49.20	0.01	-	-	0.45	0.00	100.0		66.34
LOR	6L	1	A	0.484	0.003		-0.032	0.003		49.68	0.02	-	-	0.38	0.00	100.0		11.78
VBF	2L	1	A	0.468	0.001		-0.005	0.001		49.04	0.01	2.79	0.01	-	-	100.0		39.84
VBF	6L	1	A	0.483	0.002		-0.034	0.002		49.56	0.02	2.26	0.03	-	-	100.0		7.55
xVBF	2L	1	A	0.467	0.001	0.128	-0.004	0.001	0.128	49.04	0.01	2.51	0.02	-	-	100.0		16.64
xVBF	6L	1	A	0.482	0.002	0.101	-0.033	0.002	0.101	49.57	0.02	2.03	0.03	-	-	100.0		4.65
LOR	2L	2	A	0.479	0.002		-0.002	0.002		50.43	0.02	-	-	0.30	0.00	53.5	1.0	24.87
LOR	2L	2	B	0.447	0.002		-0.008	0.002		47.08	0.30	-	-	0.36	0.01	46.5	1.1	
LOR	6L	2	A	0.493	0.003		-0.030	0.003		50.58	0.03	-	-	0.27	0.01	56.8	2.4	5.06
LOR	6L	2	B	0.456	0.005		-0.045	0.005		47.78	0.07	-	-	0.32	0.01	43.2	2.5	
VBF	2L	2	A	0.544	0.003		-0.043	0.003		49.63	0.02	2.06	0.03	-	-	47.1	0.6	12.98
VBF	2L	2	B	0.361	0.004		0.037	0.004		48.13	0.04	3.43	0.04	-	-	52.9	0.6	
VBF	6L	2	A	0.532	0.004		-0.052	0.004		50.04	0.04	1.60	0.05	-	-	53.4	1.6	2.66
VBF	6L	2	B	0.366	0.010		-0.009	0.008		48.28	0.12	3.27	0.10	-	-	46.6	1.6	
xVBF	2L	2	A	0.487	0.005	0.124	-0.003	0.002	0.124	50.11	0.04	1.51	0.07	-	-	54.8	4.1	3.20
xVBF	2L	2	B	0.424	0.004	0.133	-0.012	0.003	0.133	46.81	0.39	2.79	0.17	-	-	45.2	4.1	
xVBF	6L	2	A	0.500	0.006	0.099	-0.032	0.003	0.099	50.18	0.04	1.35	0.08	-	-	63.5	4.4	1.14
xVBF	6L	2	B	0.405	0.011	0.103	-0.055	0.010	0.103	47.11	0.51	2.90	0.25	-	-	36.5	4.4	
LOR	2L	3	A	0.478	0.002		0.003	0.002		50.99	0.03	-	-	0.27	0.00	39.2	1.2	11.84
LOR	2L	3	B	0.466	0.002		-0.013	0.002		48.52	0.03	-	-	0.26	0.01	37.0	1.7	
LOR	2L	3	C	0.426	0.004		-0.003	0.040		45.42	0.05	-	-	0.32	0.01	23.7	1.1	
LOR	6L	3	A	0.491	0.004		-0.025	0.004		51.02	0.05	-	-	0.24	0.01	43.7	2.8	2.60
LOR	6L	3	B	0.480	0.004		-0.045	0.004		48.95	0.05	-	-	0.22	0.01	33.2	3.8	
LOR	6L	3	C	0.422	0.010		-0.041	0.010		46.15	0.12	-	-	0.31	0.02	23.1	2.3	
VBF	2L	3	A	0.431	0.005		0.074	0.005		50.46	0.05	1.53	0.08	-	-	22.9	2.0	5.73
VBF	2L	3	B	0.535	0.005		-0.075	0.005		49.18	0.04	2.42	0.03	-	-	45.2	1.7	
VBF	2L	3	C	0.354	0.007		0.043	0.006		46.61	0.30	3.22	0.15	-	-	31.8	2.0	
VBF	6L	3	A	0.460	0.010		0.057	0.012		50.52	0.09	1.32	0.13	-	-	24.8	3.6	1.28
VBF	6L	3	B	0.523	0.010		-0.100	0.011		49.75	0.07	1.85	0.07	-	-	45.4	3.3	
VBF	6L	3	C	0.373	0.014		-0.014	0.012		46.78	0.57	3.18	0.20	-	-	29.8	3.8	
xVBF	2L	3	A	0.481	0.008	0.127	0.020	0.021	0.127	51.28	0.18	0.55	0.42	-	-	19.0	11.0	2.33
xVBF	2L	3	B	0.490	0.006	0.121	-0.018	0.005	0.121	49.11	0.55	1.51	0.36	-	-	42.0	11.0	
xVBF	2L	3	C	0.409	0.008	0.131	0.000	0.005	0.131	46.59	0.40	3.07	0.15	-	-	38.7	8.6	
xVBF	6L	3	A	0.501	0.009	0.111	-0.018	0.025	0.111	50.65	0.15	0.94	0.37	-	-	42.0	18.0	0.86
xVBF	6L	3	B	0.481	0.012	0.074	-0.066	0.013	0.074	48.74	1.20	1.74	0.60	-	-	34.0	20.0	

553

---

xVBF 6L 3 C 0.373 0.027 0.098 -0.014 0.022 0.098 46.28 0.82 3.65 0.38 - - 24.0 10.0